The NHXM observatory

Tagliaferri, Gianpiero; Hornstrup, Allan; Huovelin, J.; Reglero, V.; Romaine, S.; Santangelo, A.; Stewart, G.

Published in:
Experimental Astronomy

Link to article, DOI:
10.1007/s10686-011-9235-4

Publication date:
2012

Document Version
Publisher's PDF, also known as Version of record

Exp Astron
DOI 10.1007/s10686-011-9235-4

ORIGINAL ARTICLE

The NHXM observatory

Gianpiero Tagliaferri · A. Hornstrup · J. Huovelin · V. Reglero · S. Romaine · A. Rozanska · A. Santangelo · G. Stewart · Instruments & Ground Segment Team · Science Team

Received: 30 March 2011 / Accepted: 23 June 2011

Instruments & Ground Segment team: R. Ambrosi, A. Argan, G. Austin, M. Barbera, S. Basso, R. Bellazzini, A. Brez, C. Budtz-Jørgensen, A. Bulgarelli, R. Campana, O. Catalano, E. Cavazzuti, J. Chappel, E. Chen, F. Christensen, O. Citterio, M. Civitani, A. Collura, P. Connell, E. Costa, V. Cotroneo, G. Cusumano, E. Del Monte, Y. Evangelista, C. Eyles, C. Fiorini, M. Fiorini, G. Fraser, P. Giommi, A. Giuliani, P. Gorenstein, I. Hutchinson, J. Kolodziejczak, S. Korpela, N. La Palombara, G. La Rosa, F. Lazzarotto, M.C. Maccarone, G. Malaguti, S. Mereghetti, T. Mineo, F. Muleri, P. Orleanski, G. Pareschi, M. Pinchera, C. Pittori, L. Raimondi, B. Ramsey, A. Rashevski , J.M. Rodrigo, A. Segreto, P. Soffitta, D. Spiga, C. Tenzer, J. Torrejon, M. Trifoglio, M. Uslenghi, A. Vacchi, D. Willingale, G. Zampa

Science team: F. Fiore, G. Matt, M. Abramovicz, F. Aharonian, D.M. Alexander, R. Aloisio, G. Amelino-Camelia, L. Ballo, R. Bandiera, X. Barcons, T. Belloni, S. Bianchi, F. Bocchino, J. Bookbinder, V. Braito, N. Brandt, S. Brandt, L. Brenneman, G. Brunetti, N. Bucciantini, S. Campana, A. Capetti, M. Cappi, F.J. Carrera, J. Chenevez, A. Comastri, P. Coppi, S. Covino, B. Czerny, M. Dadina, R. Della Ceca, D. De Martino, M. Del Santo, T. Di Salvo, I. Donnarumma, M. Dovciak, M. Elvis, S. Fabiani, L. Feretti, V. Ferrari, A. Franceschini, M. Garcia, F. Gastaldello, I. Georgantopoulos, G. Ghirlanda, G. Ghisellini, R. Goosmann, P. Grandi, N. Grosso, P. Hakala, R. Hickox, G. Israel, M. Kadler, V. Karas, D. Lai, A. Laor, M. Limongi, A. Maggio, L. Maraschi, S. Mathur, G. Micela, S. Molendi, S. Murray, L. Natalucci, J. Nevalainen, N. Omodei, J. Osborne, M. Ostrowski, L. Pacciani, D. Patnaude, D. Perez-Ramirez, C.G. Perola, P. Petrucci, E. Piconcelli, D. Porquet, J. Poutanen, A. Ptak, S. Puccetti, M. Razzano, J. Reeves, G. Risaliti, N. Robba, T. Roberts, H. Rottgering, M. Salvati, B. Sanchez, S. Sciortino, G. Setti, P. Severgnini, L. Sidoli, M. Sikora, P. Slane, R. Smith, G. Spandre, D. Swartz, A. Szymkowiak, F. Tavecchio, A. Tiengo, P. Tozzi, A. Treves, G. Trinchieri, R. Turolla, C.M. Urry, S. Vercellone, A. Vikhlinin, J. Vrtliek, B. Warwick, N. Westergaard, A. Wolter, D. Worrall, K. Wu, G. Zamorani, L. Zampieri, A. Zdziarski

G. Tagliaferri (✉)
INAF, Osservatorio Astronomico di Brera, via Bianchi 46, 23807 Merate, Italy
e-mail: gianpiero.tagliaferri@brera.inaf.it

A. Hornstrup
DTU-space, Juliane Maries Vej 30, DK-2100 Copenhagen, Denmark

Published online: 22 July 2011

Abstract Exploration of the X-ray sky has established X-ray astronomy as a fundamental astrophysical discipline. While our knowledge of the sky below 10 keV has increased dramatically (~8 orders of magnitude) by use of grazing incidence optics, we still await a similar improvement above 10 keV, where to date only collimated instruments have been used. Also ripe for exploration is the field of X-ray polarimetry, an unused fundamental tool to understand the physics and morphology of X-ray sources. Here we present a novel mission, the New Hard X-ray Mission (NHXM) that brings together for the first time simultaneous high-sensitivity, hard-X-ray imaging, broadband spectroscopy and polarimetry. NHXM will perform groundbreaking science in key scientific areas, including: black hole cosmic evolution, census and accretion physics; acceleration mechanism and non-thermal emission; physics of matter under extreme conditions. NHXM is designed specifically to address these topics via: broad 0.5–80 (120) keV band for imaging and spectroscopy; 20 arcsec (15 goal) Half Energy Width (HEW) angular resolution at 30 keV; sensitivity limits more than 3 orders of magnitude better than those available in present day instruments; broadband (2–35 keV) imaging polarimetry. In addition, NHXM has the ability to locate and actively monitor sources in different states of activity and to repoint within 1 to 2 h. This mission has been proposed to ESA in response to the Cosmic Vision M3 call. Its satellite configuration and payload subsystems were studied as part of previous national efforts permitting us to design a mature configuration that is compatible with a VEGA launch already by 2020.

Keywords Missions · X-ray imaging · X-ray polarimetry · Cosmology · Black-holes · Compact objects · Accretion physics · Acceleration mechanism · Non-thermal emission

J.Huovelin
Department of Physics, University of Helsinki,
P.O. Box 48, 00014, Helsinki, Finland

V. Reglero
IPL, University of Valencia, P.O. BOX 22085, 46071 Valencia, Spain

S. Romaine
SAO-CfA, 60 Garden St., Cambridge, MA 02138-1516, USA

A. Rozanska
N. Copernicus Astronomical Center, Bartycka 18, 00-716, Warsaw, Poland

A. Santangelo
IATT, University of Tübingen, Sand 1, 72076, Tübingen, Germany

G. Stewart
Department of Physics and Astronomy, University of Leicester, Leicester, LE1 7RH, UK

1 Introduction

The dramatic—billion-fold—increase in sensitivity of soft X-ray observatories, from the dawn of X-ray astronomy in the early 1960s to today's space facilities, has led to the largely unexpected detection of high-energy radiation from objects of all scales in the Universe. Virtually every class of astrophysical object, from ultra-compact BHs and NSs, through normal stars, and star formation regions to diffuse hot plasma pervading galaxies and clusters of galaxies has been found to emit X-rays. Even planets and comets are known to be X-ray sources. Thanks to these advances we know the three primary physical processes behind the emission of energetic radiation: accretion physics, astrophysical shocks and particle acceleration. Thermal and non-thermal components can be cleanly separated above 10 keV, but unfortunately more than four orders of magnitude separate the sensitivity in hard X-rays achieved by BeppoSAX, Suzaku, INTEGRAL and Swift from that achieved by X-ray telescopes below 10 keV. In addition, X-rays are usually emitted in highly aspherical geometries so that high degrees of polarisation are expected (in contrast to the optical band dominated by stellar processes). However, although X-ray polarimetry was born in the 1970s, advancements have so far been marginal.

A fine hard X-ray imaging and polarimetry observatory will allow, for the first time, to uncover the bulk of accretion power in the Universe, the physics of accretion and of "cosmic accelerators". To this end we have designed a new mission, NHXM, that will have on board four Mirror Modules (MM) with good imaging capability in the band 0.3–80 (goal 120) keV. Three MM are coupled with three spectral imaging cameras, with two detection layers plus an anticoincidence system, sensitive in the full mirror band. One MM is coupled with the polarimetry imaging camera, with two polarimetric detectors to cover the 2–35 keV band. There is one Wide Field X-Ray Monitor (WFXRM) sensitive in the 2–50 keV band to find active and transient sources.

2 Scientific objectives

2.1 Black hole cosmological evolution and accretion physics

Accretion onto compact objects (stellar or SMBHs, NSs, white dwarfs) provides a very efficient way to convert gravitational energy into radiation. It is indeed the dominant process producing X-rays in the Universe. Thanks to the advent of grazing incidence mirrors, first in soft X-rays ($E < 3$ keV with Einstein, EXOSAT and ROSAT) and later on up to 10 keV (with ASCA, BeppoSAX, XMM-Newton and Chandra), it has been possible to prove that the Cosmic X-ray Background (CXB) is due to the integrated contribution of accreting SMBHs shining in AGN. It peaks at $\sim$30 keV (Fig. 1) but in this band only 1–2% of its energy density is resolved into discrete sources by INTEGRAL and Swift. The CXB can be viewed as the integral over cosmic time of the accretion processes taking place during the growth, through mass

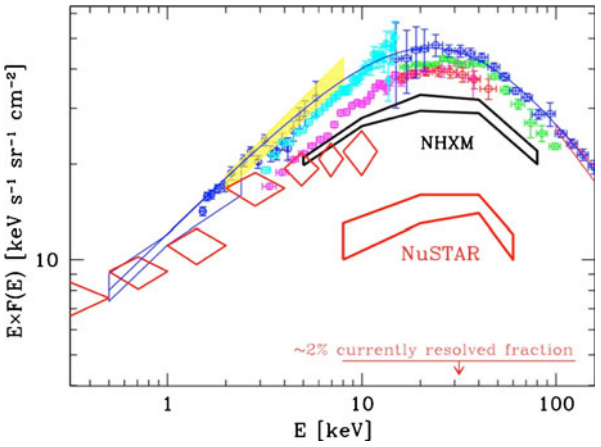

Fig. 1 CXB spectrum measured by various experiments. *Red diamonds* fraction of the CXB resolved into discrete sources by Chandra and XMM-Newton. NHXM will resolve ≥70% of the CXB where it peaks, finding these elusive sources up to z ∼ 2. The *black region* mark the CXB fraction resolved by NHXM in 1 Ms (*lower envelope*) and 2 Ms (*upper envelope*). We also report in red the fraction resolved by NuSTAR at its confusion limit (reachable in ∼300 ks) accounting for the statistical uncertainty on the number of sources in 10 such NuSTAR observations

accretion, of SMBHs. It is probably produced at $z \sim 1$, meaning that most AGN power is emitted at ∼60 keV or more. How this hard emission is produced, the exact modes in which accretion occurs, how the accreting matter is distributed, and the complex interplay between the AGN power and their host galaxies, are all still poorly known. NHXM will resolve most of the CXB at its peak energy density, shedding light on the physics of accretion and the emission mechanisms.

BH census and cosmological evolution Many AGN synthesis models for the CXB predict a large volume density of Compton Thick (CT) AGN; however, a more complex AGN X-ray spectrum at $z > 1$ can also produce the observed CXB [21]. To break the degeneracy we need direct identification of CT AGN, only possible with sensitive hard X-ray observations.

Highly obscured AGN may reveal a key phase in galaxy evolution corresponding with the onset of AGN feedback. AGN activity is thought to be triggered by channeling of matter toward the galaxy nucleus, where it can accrete onto a central SMBH. Unfortunately, our current understanding of the interplay between the AGN and the galaxy (i.e. feedback processes) is still rather primitive. A breakthrough would be provided by the direct observation of *objects where feedback is in action,* i.e. young AGN still in the process of blowing away their cocoon of dust and gas. To discover a significant number of new sources we need to resolve a fraction of the CXB at E > 10 keV higher than that currently resolved at 5–10 keV (∼50%). This is one of the main goals of NHXM and it is not achievable by NuSTAR (a NASA satellite to

be launched in 2012 with imaging capability in the band 7–80 keV). Figure 2 shows a simulation of a 2 Ms NHXM observation of an area of the Chandra Deep Field South (CDFS) in the 10–40 keV band. NHXM can detect about 40 sources in this field down to a flux limit of 3×10^{-15} cgs (with 8–10 CT AGN, 3–4 of which are at $z > 1$), implying that about 75% of the 10–40 keV CXB will be resolved. For comparison, NuSTAR can detect only 8–10 sources, with just 1 CT AGN.

Accretion Physics: AGN The broadband emission observed in AGN depends on the complex interplay between a cold accretion disk and a hot corona of ionized plasma. Reflection-transmission from cold-warm matter located far from the nucleus further complicates the picture. Broadband X-ray spectroscopy and simultaneous polarimetry provide the most direct information on the nature of the primary component originating from the hot corona, and the hard reflection component coming from circum-nuclear matter (accretion disk and/or torus), allowing for a comprehensive study of the disk/corona system.

The primary emission of AGN is due to Comptonization, but the origin and geometry of the hot corona are largely unknown. For bright sources NHXM will precisely measure the continuum up to 70–80 keV, allowing the determination of the high-energy cut-off to within 10% (even if it is at 200 keV), in a 100 ks observation of a bright Seyfert 1 galaxy. This strongly constrains the corona temperature, while with the polarimetric measurement we have the possibility to determine the corona geometry [18].

The reflection component is expected to be highly polarised, a characteristic that can be used to constrain the torus geometry. In the archetypal CT AGN, NGC 1068, IR interferometry suggests a surprising misalignment between the

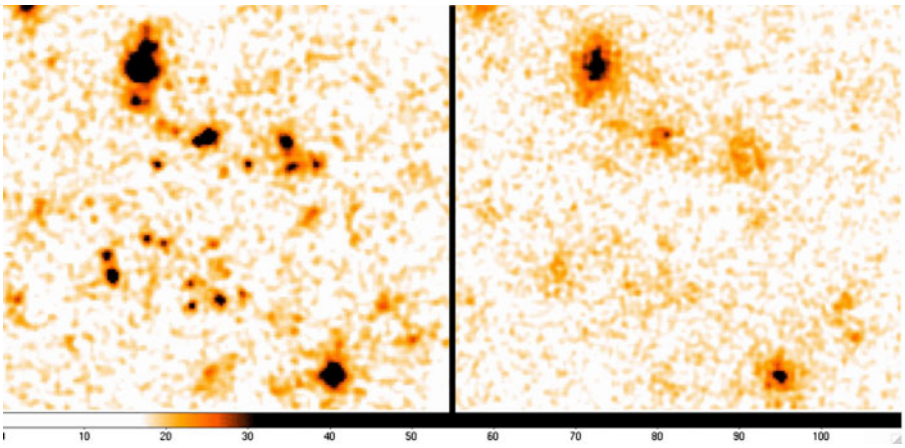

Fig. 2 2 Ms NHXM (*left*) and NuSTAR (*right*) 10–40 keV simulations of a ∼10′ region of the CDFS, assuming a PSF with 15″ HEW on axis for NHXM and 45″ HEW for NuSTAR. Two input source catalogs have been used: (1) sources detected by Chandra in the 2–10 keV band [10]; (2) the candidate highly obscured AGN selected in the mid-infrared by Fiore et al. [7]

torus axis and the ionization cone of about 20° [15]. X-ray polarimetry may confirm or disprove these important results (see [8], for details). For a, rather conservative, polarisation degree of 10% (20%), the polarisation angle can be measured in 300 ks with an error of 5° (2.5°) in the 6–35 keV band.

Accretion physics: X-ray binaries Accretion physics can be studied in detail over shorter time scales in nearer and therefore brighter systems, namely Galactic XRBs, where a compact object accretes matter from a companion star. The broadband spectroscopic and polarimetric capabilities of NHXM can study the interplay (and its time evolution) between the accretion disc, the hot corona and the jet. The WFXRM will allow us to study the evolution of transient sources and to catch systems in extreme and rare states.

The broadband monitoring of the state transitions (quiescence → hard → soft → quiescence, through different intermediate states) is crucial because it signifies the evolution and interplay between the disc/corona system and the onset of relativistic jets [5], while time-resolved spectroscopy and polarimetry are crucial to study the evolution of thermal and non-thermal components.

Accretion physics: the Galactic center and the galactic background Most galaxy nuclei in the local Universe lack significant activity, with very low accretion rates onto their central SMBHs. The SMBH hosted in the Galactic Center and coincident with the radio source SgrA*, is no exception. Its luminosity is many orders of magnitude ($\sim 10^8$–10^9) lower than the Eddington luminosity for a BH of $4 \times 10^6\ M_{Sun}$. Chandra and XMM-Newton have revealed the daily occurrence of X-ray flares from SgrA*, likely originating very close to the BH event horizon. The broad-band study of these X-ray flares is crucial to understand the accretion and ejection processes at work in such quiescent BHs, to identify the emission mechanism and accretion mode. Polarimetric observation of the Galactic Centre region can solve the problem of the origin of the X-ray emission observed from giant molecular clouds in this area. This emission is likely due to reflection of an external illuminating source, and since there is not a sufficiently bright source in the surroundings, it has been proposed that Sgr B2 is echoing past emission from Sgr A*. Polarimetry can prove this (see Fig. 3), because a polarisation vector perpendicular to the line connecting the molecular cloud and the illuminating source is expected. This observation can confirm that the BH in our own Galaxy was much more active in the past (a few hundred years), and hence demonstrate that inactive galaxies may be re-ignited.

2.2 Acceleration mechanisms

Winds and jets from AGN can propagate for extremely long distances (up to Mpc), and are responsible for injecting energy in to interstellar matter in galaxies and intra-cluster gas. However, despite a wealth of observations on this feedback process (particularly in galaxy clusters), the physics behind the formation of jets and knowledge of their emission mechanisms remain quite

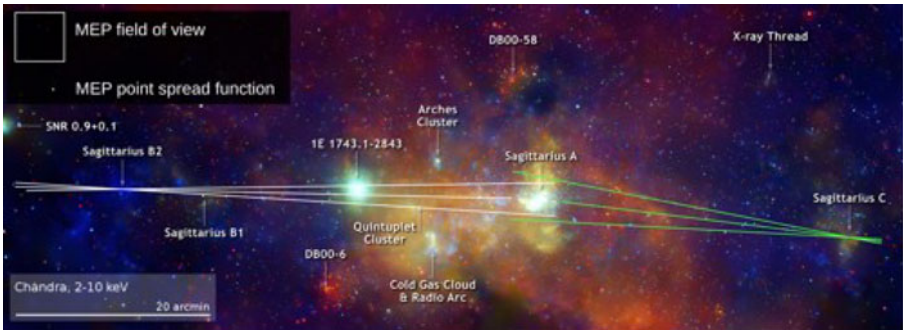

Fig. 3 SgrA*, SgrB2, SgrB1 and SgrC region as seen by Chandra. Overlaid are the angular constraints on the source illuminating Sgr B2 and Sgr C, that can be derived with an observation of the Medium Energy Polarimetric camera (see payload section)

poorly understood. Similarly, cosmic rays are believed to be accelerated in shocks, both in SNR and in the intra-cluster medium. However, the details of this process are still very much a mystery. Sensitive broadband imaging, spectroscopy and polarimetry can provide breakthroughs on all these problems.

Blazar and microquasar jets The process of jet formation following accretion from the disk is revealed in the erratic flaring activity and plasma ejection of microquasars. These ejection phenomena can be directly associated with the status of the system before and after the flare. In radio-loud AGN, timescales are much longer, but broadband spectroscopy and polarimetry can very efficiently separate jet emission, which is most likely due to synchrotron/inverse Compton (IC) processes, from accretion disk emission (including its X-ray corona and reflection). Blazars show two emission peaks, associated with synchrotron and IC processes. If due to synchrotron, X-rays must be highly polarized. The combination of X-ray and optical-infrared polarimetry can then assess whether the same electron population gives rise to the emission in both bands, i.e. we can directly probe the jet structure. If X-rays are due to IC, the degree of polarisation depends on whether the seed photons are synchrotron or from the disk (e.g. [11]). In the first case the polarisation angle of the synchrotron and IC emission should be the same. Multi-band polarimetry can therefore solve the long-standing issue of the nature of the jet seed photons. In the most powerful blazars the optical emission comes from accretion, and for these we can measure the BH mass and the accretion rate and thus compare jet and accretion powers. Since powerful blazars are the most luminous hard X-ray sources above 20–50 keV, we can find them up to large redshift with the WFXRM (see Fig. 4), providing a census of jetted systems of large BH masses above $z \sim 4$. Finding high mass BHs in even a few blazars (aligned) implies the existence of many more BH (in misaligned fainter objects) with the same mass.

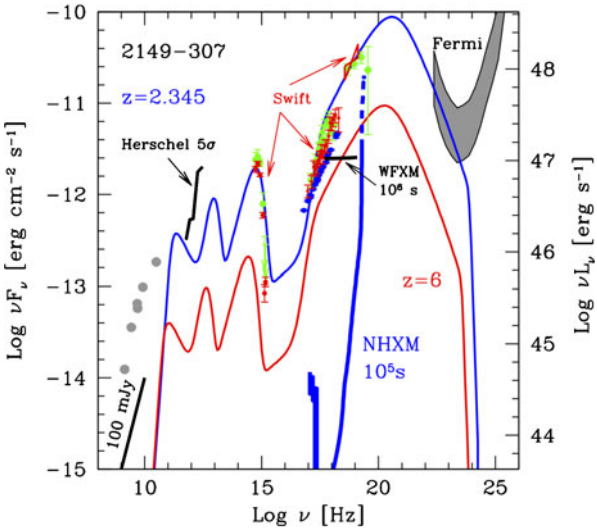

Fig. 4 SED of 2149-307, a powerful Flat Spectrum Radio Quasar detected in the hard X-ray band by BAT. In these sources NHXM can observe the rising part of the high-energy bump, where most of the power is released, providing accurate spectral and polarimetric variability information on timescales of few thousand sec. The *red curve* is the model reproducing the same SED at z = 6, still well within the NHXM capability. The *thick blue line* provides the NHXM sensitivity in 100 ks

Acceleration mechanisms in clusters of galaxies AGN jets and outflows can strongly affect the intra-cluster medium of clusters of galaxies, releasing energy there in the form of accelerated particles and shock waves. Shocks with typical Mach numbers 2–4 are produced during the assembly of clusters of galaxies through merging of subunits, when a large quantity of energy is redistributed between the main intra-cluster medium components: hot baryons, relativistic particles and magnetic fields. Recent radio observations suggest that diffusive shock acceleration operates on clusters of galaxies similarly to SNRs, and are capable of producing energetic cosmic rays [23]. IC scattering of the CMB on the same relativistic electrons can produce non-thermal X-rays. The NHXM unique broadband spectral and imaging quality and sensitivity allow discovering and studing a large number of shocks up to the virial radius, mapping the heating history of the cosmic component that includes the largest fraction of the baryons at $z < 1$. NHXM can also study the spectrum of non-thermal IC emission, disentangling the different acceleration mechanisms (merger shocks vs. hadronic collisions) (see Fig. 5).

Acceleration mechanisms in supernova remnants The process of particle acceleration can be conveniently studied in much more detail in nearer and brighter systems such as SNRs. The synchrotron radiation from relativistic e^- is a diagnostic tool for the mechanism of diffusive acceleration in SNR shocks, believed to be the source of the cosmic rays up 10^{15} eV. While thermal emission is usually confined to soft X-rays, synchrotron (as well as non-thermal bremsstrahlung) emission is best studied at higher energies, using high-quality spatially resolved broadband spectroscopy and polarimetry, all features that make NHXM ideal. Measuring the cut-off frequency provides the maximum energy of electrons (if the magnetic field is known), while the azimuthal

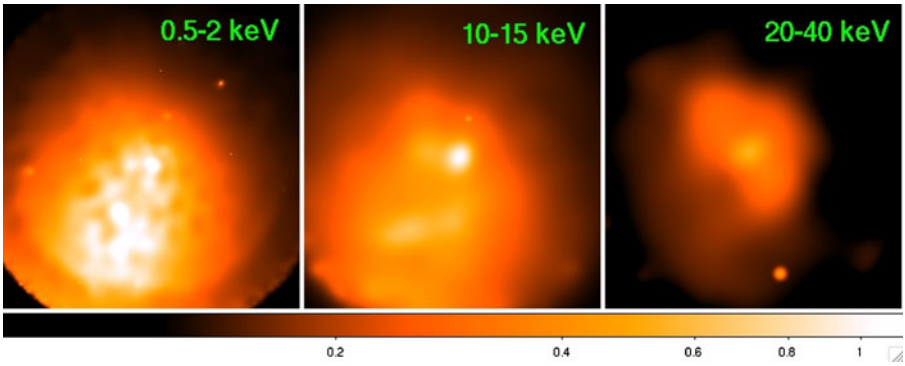

Fig. 5 200 ks NHXM simulations of Abell2256 in three bands. The simulation includes thermal emission (as measured by XMM-Newton), and a non-thermal component co-spatial with the radio relic located in the 5 × 5 arcmin northern region, with a 20–80 keV flux of 5×10^{-12} cgs and $\alpha_E = 0.8$ for this component

variation of this maximum energy along the SNR shock and of the polarisation will provide its dependence on the ambient magnetic field orientation. In addition, a comparison of hard X-ray and TeV images can provide information on ion acceleration. Depending on their relative morphologies and fluxes, TeV emission can be dominated by either IC radiation from the same electrons emitting synchrotron X-rays, or by hadronic emission through $\pi +$ decay.

The best studied case for SNR non-thermal emission is SN 1006, the archetypal non-thermal shell-type SNR. NHXM could detect radiation up to ∼30 keV in its brighter X-ray limbs, measuring both the synchrotron spectral index and the cut-off energy. A comparison with the radio spectral index then allows a search for deviations from the power-law spectrum, testing the shock modification level. While in the brightest remnants like CAS-A or Tycho NHXM can identify the regions of hard X-ray emission and measure polarisations of the order of a few % in ∼10 angular bins. For these extended objects the imaging capability of NHXM will provide a dramatic improvement with respect to the non-imaging capabilities of GEMS (a NASA satellite dedicated to X-ray polarimetric measurements but without imaging capability, to be launched in 2014–2015).

Another promising field of research is the study of the 67.9 and 78.4 keV emission lines of ^{44}Sc, from the ^{44}Ti radioactive decay chain in young SNRs. This isotope is created in all types of SNe: models predict values between 8×10^{-6} and 5×10^{-5} M_{Sun} in the Type Ia SNe, and up to 3.9×10^{-3} M_{Sun} in some rare cases of He-detonation. The measured yield for Cas A (1.5×10^{-4} M_{Sun}) is higher than that predicted by spherically symmetric models, suggesting asymmetries in the explosion, easily verified by NHXM by mapping the spatial distribution of the emission.

Pulsar wind nebulae The relativistic wind of young pulsars interacts with the surrounding supernova remnant, injecting relativistic electrons and magnetic

field into synchrotron emitting wind bubbles, giving rise to PWNe. The brightest and most spectacular PWN is the Crab Nebula. PWNe are highly structured in X-rays, as shown by Chandra observations of the Crab Nebula (Fig. 6), with a jet, a torus and several rings varying on short time-scales. Broadband imaging spectroscopy and polarimetry is necessary to map the electron population near injection (and its spatially dependent spectral distribution), together with the magnetic field. A broad spectral band is also required to search for spectral steepening at higher energies at different sites. Since magnetic fields in PWN must be rather well ordered, the emission is locally highly polarized, as confirmed by radio observations. Imaging polarimetry is fundamental to probe the magnetic field topology. Since X-ray emitting electrons have short synchrotron lifetimes, X-rays provide the cleanest view of the inner regions, limiting the risk of superposition effects along the line of sight. NHXM will be able to obtain extremely accurate spectral and polarisation maps of the Crab Nebula, impossible with GEMS. When combined with existing radio and optical maps, showing quite different morphologies, a complete picture will be available, representing a benchmark for theoretical models, shedding light on the particle acceleration and propagation mechanisms. The angular resolution would also allow measuring the polarisation of the Pulsar, which in OSO-8 (and also in GEMS) is overwhelmed by the nebula.

Acceleration mechanisms in other sources The NHXM characteristic will allow us to study acceleration mechanism in many other sources. Stellar coronae represent the largest class of X-ray sources in our Galaxy. NHXM can study hard X-ray emission from quiescent and flaring coronae and the relationship with non-thermal radio emission. Quiescent X-ray emission and flares from young stellar objects in star forming regions can also been studied, which is of

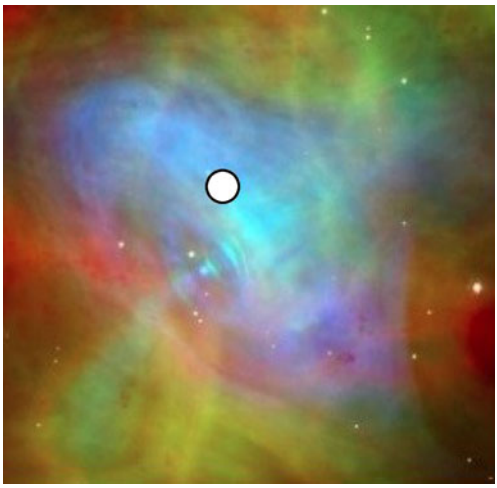

Fig. 6 Composite Chandra and HST image of the Crab nebula with overlaid the spatial resolution of NHXM polarimeter

primary importance for the effects on the circumstellar environment and hence on the star and planetary formation processes.

While the Lorenz factor in Blazar jets can reach a value of several tens, it can reach a value of thousands in Gamma Ray Burst (GRB) jets, making these objects the most powerful accelerators in the Universe. Despite the enormous progress that has occurred in the last 10 years, the GRB phenomenon is still far from being fully understood. NHXM can study the afterglow emission above 10 keV, a field almost completely unexplored, and measure the polarisation of the afterglow emission, probing GRB jets. The WFXRM can detect and localize ∼30 GRB/year, 20% of which are expected at $z > 5$. GRBs can be repointed on 1 to 2 h timescale, allowing broadband spectroscopy and sensitive polarimetry.

2.3 Physics of matter under extreme conditions

Broadband X-ray spectroscopy and polarimetry can probe matter under extreme conditions, and in so doing test fundamental physical theories.

Strong gravity effects around black holes and neutron stars General Relativity (GR) and relativistic accretion disks can be investigated through both broadband spectroscopy and polarimetry. Distortion of the iron line profile, caused by GR effects, has been observed in AGN, Galactic BH systems, and recently also in accreting NSs. Measurements of BH spin (a key parameter to understand BH evolution) have been published for both Galactic BHs and AGN. The debate on the relativistic nature of these lines is however still hot, as some authors claim that they are, at least in AGN, simply an artifact of complex absorption (see [22, 25]). While the two models are often degenerate below 10 keV, their extrapolations to higher energies are different, and easy to distinguish by NHXM. In Galactic systems, the broadening of the line is sometimes attributed to Comptonization. Since in this scenario the line should be polarized, NHXM will open an entirely new opportunity for observational tests.

Even when the relativistic disk nature of the line is accepted, a robust determination of the disk and BH parameters is hampered by systematic uncertainties. A second method has been already employed to estimate theBH spin in Galactic BH systems in the high state, i.e. the fitting of the thermal continuum. Results obtained by the two methods, while very precise on statistical grounds, often contradict each other [13, 17], indicating large systematic uncertainties. The suite of instruments of NHXM is ideal to reduce these uncertainties. Thanks to the broadband spectroscopy, an excellent determination of the continuum is possible, permitting a reliable confirmation of the relativistic nature of the iron line profiles, and a robust determination of the disk and BH parameters. When applied to the disk thermal continuum method, any non-thermal, hard X-ray contribution can be properly subtracted. In addition, polarimetry provides a third, independent method. GR effects

rotate the polarisation angle of the radiation emitted from the disk, the amount of rotation increasing with decreasing disk radii.

As the disk temperature has a similar radial dependence, an energy-dependent rotation of the polarisation angle is produced. Figure 7 shows the result from the simulation of a 200 ks observation of the X-ray binary GRS1915+105, demonstrating that the spin can be measured with high precision. Once the three methods are tested, calibrated and validated in Galactic BH systems, it will be possible to apply the iron-line method (the only available method in this case) with confidence to SMBHs.

Strong, very strong and extreme magnetic fields X-ray emission in white dwarfs/NSs may be heavily affected by a strong (10^{6-8} G), very strong or extreme (10^{12-15} G) magnetic field. The simultaneous X-ray broad-band and polarimetric capability of NHXM has the unique potential of studying in detail the magnetic field properties and accretion mechanism around these compact magnetic sources. We will also be able to study cyclotron lines expected above 10 keV, with both hard X-ray spectroscopy and polarimetry.

Soft Gamma Repeaters (SGRs) and Anomalous X-ray Pulsars host a hyper-magnetized, isolated NS, or *magnetar* [4]. The surface dipolar fields are substantially in excess of the quantum critical limit ($B_{QED} = 4.4 \times 10^{13}$ G). Magnetars are likely powered by the huge magnetic energy stored in the NS interior. They are characterized by the erratic emission of short (<1 s), intense ($L_X \sim 10^{40}$ erg/s) X-ray bursts. Three SGRs have also displayed much more energetic events, so-called "Giant Flares", during which up to 10^{47} erg were emitted in about a second (see [12]). NHXM is expected to provide fundamental contributions to their understanding. The temporal behaviour (both periodic and aperiodic) will be studied over a very broad band, shedding light on the emission mechanism and the energy budget. The broad-band polarimetric capability will add invaluable information on the radiative transfer in extreme magnetic fields. The polarisation degree is expected to

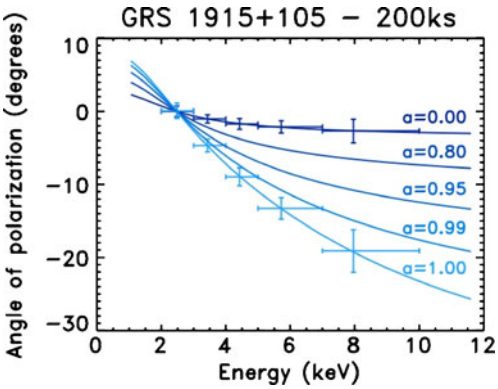

Fig. 7 NHXM simulations of the polarisation angle measurements (α) vs. energy in GRS1915+105 for different Bh spin

increase with energy, and therefore it will be best studied with the MEP. Very important is the possibility of inferring the magnetic field and/or the distance of magnetars by studying the so-called intermediate flares. During these flares the emission reaches the "magnetic Eddington luminosity", and peaks in hard X-rays [9]. This activity lasts for few hours, therefore a fast trigger (allowed by the WFXRM) and repointing capability is required.

3 Mission profile

The NHXM mission, including the payload accommodation and satellite properties, has been studied in a dedicated industrial study by ThalesAleniaSpaceItaly. The NHXM satellite is made of the service module platform, accommodating the four mirrors modules, and the Instrument Platform accommodating the focal plane assembly. The Instrument Platform will be put at the 10 m focal length distance by a deployable truss, after the satellite has been placed in orbit. Therefore, NHXM can be launched in a very compact configuration allowing for the use of a smaller fairing launcher.

The requirement of a very low and stable background count rate dictates the need for a Low Equatorial Orbit (LEO). As shown by the experience of two very successful hard-X-ray missions, BeppoSAX and Swift, a circular nearly equatorial (inclination $<5°$) orbit, at 600 km mean altitude with an orbital period of 95 min, guarantees a very stable and low background environment. This choice will ensure:

- remaining below the inner Van Allen radiation belt, avoiding passages within regions of trapped charged particles;
- short passages over the edge of the South Atlantic Anomaly;
- minimization of the "soft proton flares" problems;
- $\sim$ 10 min/orbit (2.5 h/day) visibility from an equatorial Ground Station.

NHXM will be operated as an observatory following standard rules in terms of AO, data right, data distribution, etc. Still we envisage that there must be a core program to guarantee that the scientific key objectives of the mission are met. The "envelope" of this core program should be defined by a NHXM Scientific Working Group. In addition, NHXM has the ability to locate and actively monitor sources in different states of activity, permitting their detailed study. When a new bright source is detected by the WFXRM, its position is passed to the AOC in $\leq$1 min and, if feasible, the satellite autonomously repoints to this target, on a time scale of $\leq$1–2 h after the trigger. The new source will be observed for a pre-defined amount of time depending on a priority value set by the onboard software. After that the satellite will return to its previous schedule. This capability, on a much more demanding scale, has already been proven by the Swift satellite. This is not our main driver, but still is one of the parameters considered in designing the mission.

4 The payload

In Table 1 we list the technical requirements set by the NHXM scientific goals. These requirements set also the payload configuration that includes:

- 4 MMs with good imaging capability in the band 0.3–80 (0.3–120 goal) keV,
- 3 MMs are coupled with three sensitive spectral imaging cameras with two detection layers each, plus an effective anticoincidence system;
- 1 MM is coupled with two polarimetric detectors sensitive in the band 2–35 keV, composing the polarimetric imaging camera;
- 1 WFXRM sensitive in the 2–50 keV band to find active and transient sources.

and is based on development studies carried out in recent years. In some cases prototypes have already been built. Therefore we have in place a well-defined plan to develop the payload in due time and with the requested capabilities.

The mirror modules The four identical NHXM Mirror Modules (MMs) will be based on nested confocal electroformed Nickel-Cobalt alloy (NiCo) shells with Wolter I profile. The electroforming technology has already been successfully used for the Ni gold-coated X-ray mirrors of BeppoSAX, Jet-X/Swift and XMM-Newton satellites and it is now used for the mirrors of the

Table 1 NHXM scientific requirements

Parameter	Value
Energy band:	0.3–80 (120 goal) keV
FOV (at 30 keV)	$\geq$ 12 arcmin
On-axis sensitivity	$\leq 10^{-14}$ cgs ($\sim$0.5 μCrab), 10–40 keV (3σ, 1 Ms, PL-$\Gamma = 1.6$)
On-axis effective area:	$\geq$ 300 cm^2 at 0.5 keV
	$\geq$ 1,000 cm^2 at 2–8 keV
	$\geq$ 350 (500) cm^2 at 30 keV
	$\geq$ 100 cm^2 at 70 keV
	$\geq$ 20 cm^2 at 100 keV (goal)
LED background	$< 1 \times 10^{-3}$ cts s^{-1} cm^{-2} keV^{-1}
HED background	$< 2 \times 10^{-4}$ cts s^{-1} cm^{-2} keV^{-1}
Angular resolution (HEW)	$\leq$15″ (10″ goal) E $<$ 10 keV
	$\leq$20″ (15″ goal) E $<$ 30 keV
	$\leq$40″ at E = 60 keV (goal)
E/ΔE	40–50 at 6 keV; 60 at 60 keV
Polarisation sensitivity	9.7% Minimum Detectable Polarisation in 100 ks for 1 mCrab (2–10 keV) & 1.8 mCrab (6–35 keV)
Wide Field X-Ray Monitor Sensitivity	2 mCrab in 50 ks at 5 σ (2–50 keV); triggering on a 0.5 Crab source in 1 s, providing the position in $<$1 min, FOV = 2.9 sr partially coded, 0.5 sr fully coded
Absol. pointing reconstr.	3″ (radius 90%)
Mission duration	3 years + provision for at least 2 years extension

e-Rosita mission. For the NHXM mirrors, a few technological modifications will be introduced that have already been developed in the past several years. We will use *NiCo alloy* instead of pure Ni. NiCo is characterized by better stiffness and superior yield properties. We will apply *nanostructured multilayer* X-ray reflecting coatings, permitting a larger FOV and an operating range from 0.3 keV up to 80 keV and beyond. These will be sputtered onto the internal surface of the gold-coated NiCo mirror thin shells after replication from the mandrels.

Each MM is equipped with 70 (in the baseline configuration, 90 in the goal configuration) Wolter-I Mirror Shells with a focal length of 10 m and interface diameters in the range ∼390 to ∼150 mm. The general layout of a MM has been extensively studied via a Final Element Method analysis. Various auxiliary devices will be installed on each MM: a magnetic diverter to prevent background electrons reaching the detector, a thermal baffle and a thermal blanket to maintain the mirror temperature. A X-ray precollimator is optional and not foreseen in the baseline configuration. The total mass for the 4 MMs will be ∼530 kg, for the worse case (90 shells with precollimator). The effective area for three mirror modules is shown in Fig. 8 for the baseline and the goal configuration. The latter is achieved by filling the internal hole of each MM with an additional 20 mirror shells (to a minimum shell diameter of 110 mm). These shells will be fabricated via direct replication of multilayers (e.g. Pt/C/Ni) from TiN-coated superpolished mandrels [16], adding 5 kg to each MM. Several engineering models (EM) with Ni and NiCo integrated shells coated with W/Si and Pt/C multilayer films (200 bilayers) have been developed and tested at the Panter-MPE X-ray calibration facility (Fig. 9) demonstrating the feasibility with a microroughness of <4 Å [14, 20].

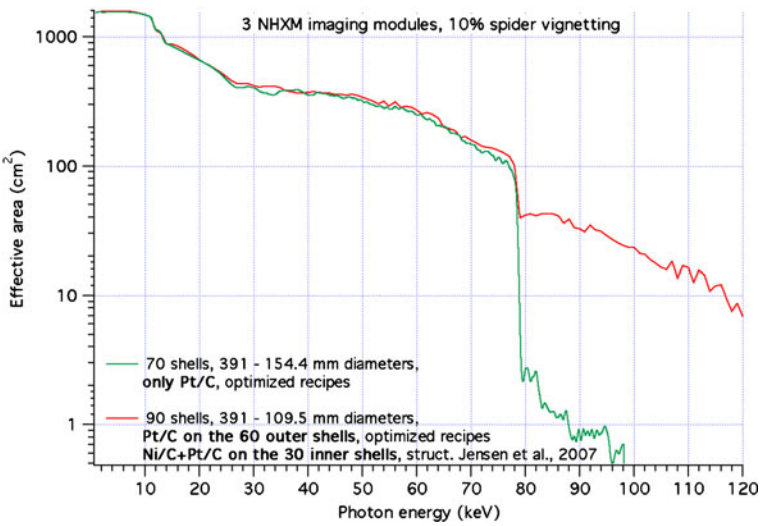

Fig. 8 Three-MM effective area (baseline and goal)

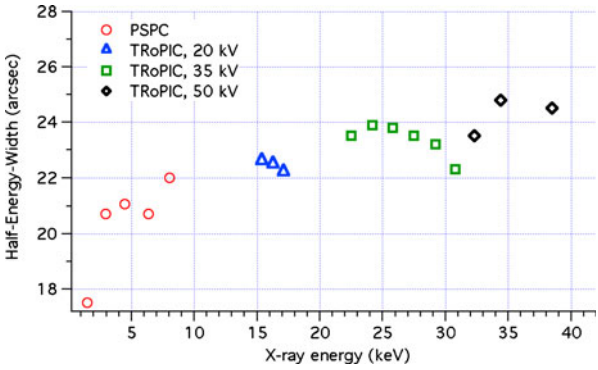

Fig. 9 HEW as a function of energy for an EM measure at the Panter X-ray facility

The three identical spectral imaging cameras X-rays focused by the mirrors enter the camera via an extended graded baffle tube, which protrudes 900 mm from the focal plane. The baffle is mechanically supported by a conical structure, mounted on the camera at the instrument platform interface plane. A door aperture sits in front of a filter wheel, which is mounted directly in front of the Low Energy Detector (LED). The door is normally closed for ground testing.

The main camera body can be evacuated to facilitate bench testing and to protect delicate filters from acoustic excitation during launch. The door is opened in orbit by venting a bellows via a high output paraffin actuated valve. A stepper-motor controlled, four-aperture filter wheel is mounted directly in front of the LED and is mechanically supported by the door chamber assembly (see Fig. 10, left panel). The filter wheel will provide an open and a closed position, one position with a medium filter and one with a calibration source. The LED and HED detectors are hosted inside two very compact detector modules that will also provide an active and passive shielding to minimise the shielding mass by being in close proximity to the detectors (see Fig. 10, right panel). The two modules will be integrated separately, allowing for independent development. The 12-arcmin FOV diameter implies a focal plane size of 4×4 cm^2. The final combined broadband flux sensitivity of three telescopes is reported in Fig. 11. The LED: as baseline we choose an e2 V CCD device thinned to ~150 μm, to ensure adequate transmission for energies above 10 keV, with a 120 μm depletion layer (goal 150 μm, i.e. fully depleted). It will have a pixel size of 100–200 μm, an acquisition rate of 10 full frames per second and a QE of 98% at 6 keV and 59% at 10 keV. Windowing mode operation will enable high-speed readout, ~50–100 s^{-1}, avoiding pileup for bright sources (with a pixel size of 100 μm we can observe a 100 mCrab source with less than 5% pileup). An alternative solution would be to use a Macropixel detector based on an active pixel sensors concept (DEPFETs) already extensively studied and characterized in the context of Simbol-X and IXO. The HED: will be mounted below the LED and will perform spectral imaging of hard X-ray photons in the 7–120 keV energy band. The HED

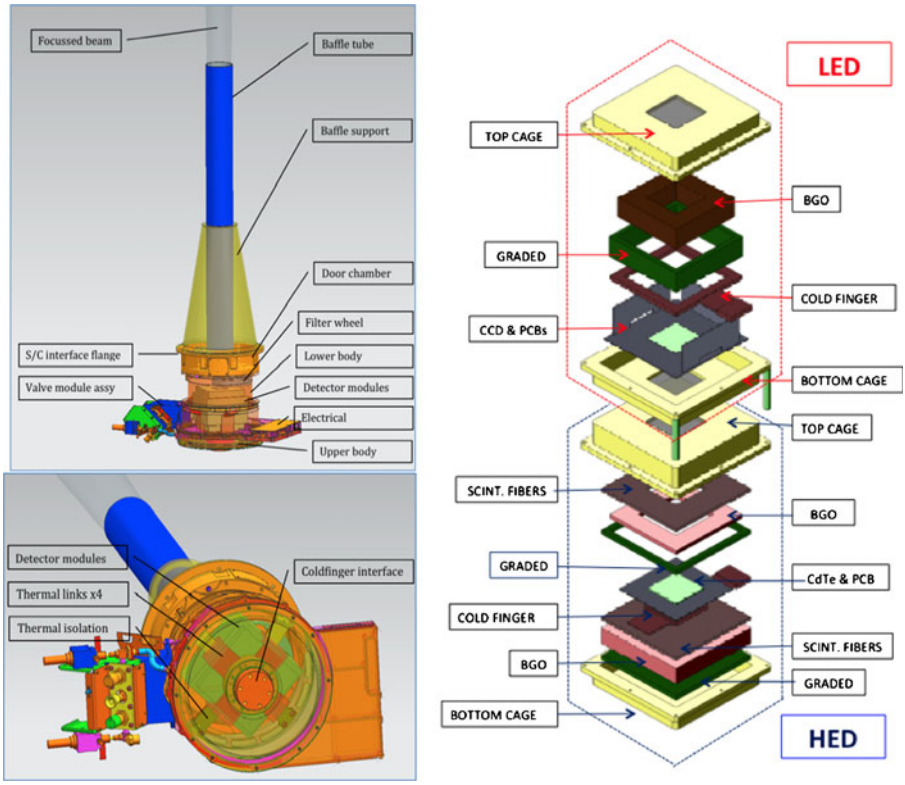

Fig. 10 *Left*: overview and inside view of a spectral imaging camera. *Right*: LED and HED modules exploded view

baseline is a 1–2 mm thick pixellated CdTe detector read out by a bump-bonded ASIC chip. The CdTe sensor is a Schottky type diode with Al contacts on the junction side. This type of configuration collects electrons at the pixels, and holes at the uniform ohmic contact on the opposite side. It can be operated at 1–2 kV bias voltage with very low leakage current (<1 pA/mm^2) with the required energy resolution, if the temperature is maintained in the -20°C to -40°C range. A first CdTe+ASIC hybrid module has already been realized. Schottky CdTe crystals with the smallest available pitch (80 μm) have been produced, according to our design and requirements (118604 hexagonal pixels over an area of 25×28 mm^2) by ACRORAD. We selected this small pixel size in order to use the same ASIC developed for the polarimetry detector and that we already had in house. For the flight configuration the HED pixel size will be in the range of 200–350 μm. The hybrid module has been obtained by bump bonding the Aluminum pads of the crystal to the pixels of a dedicated large-area ASIC. The bump-bond processing has been made by AJAT, a Finnish Microelectronics Company, successfully proving the proposed technology (99% good connections, e.g. [2]). For the NHXM configuration the active area will

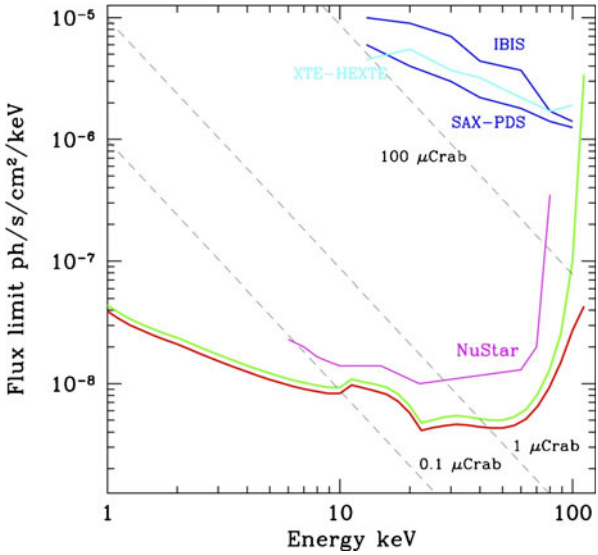

Fig. 11 NHXM broadband flux sensitivity for 1 Ms for baseline (*green*) and goal configuration (*red*). To derive these sensitivity curves we assumed for the LED and HED background the required values given in Table 1 and a $\Delta E = 2E$

be arranged as a 2×2 matrix of four CdTe-ASIC hybrids, each 20×20 mm^2 wide. As a back-up option we have identified the compound CdZnTe, already used for previous mission with hard X-ray detectors (INTEGRAL, Swift). An interesting prototype has been developed in the context of the Simbol-X project. Shielding system: passive and active shielding surrounds the detection units except for the solid angle corresponding to the optics focused beam. Scintillating fibers with an active layer of inorganic scintillator constitute the anti-coincidence system. The function of the passive shield is to absorb most of the photons and low energetic particles while the role of the active shielding is to reject the pass-through of charged particles and hard-X-/soft-γ-ray photons. For the passive shielding a graded configuration, used also for the camera baffles, is coupled with a 2 cm inorganic scintillator (BGO or CsI) and an array of plastic scintillating fibers of 1 mm of diameter (see Fig. 10). Extensive GEANT4 simulations show that the mission background requirements (see Table 1) can be meet with our configuration.

The polarimetric imaging camera Also for the polarimetric camera, at the focal plane of the fourth telescope, the goal is to cover an energy range as large as possible. The focal plane polarimeter will provide polarisation measurements simultaneously with angular, spectral and timing measurements. The instrument is based on a Gas Pixel Detector, a position-sensitive counter with proportional multiplication and a fine subdivision of the charge collecting electrode in such a way that photoelectron tracks can be accurately reconstructed and their emission direction derived [3]. The linear polarisation is determined from the angular distribution of the photoelectron tracks. The Gas Pixel Detector (GPD) is based on a gas cell with a thin entrance window, a drift gap, a charge amplification stage and a multi-anode readout plane, which is the

pixellated top metal layer of a CMOS ASIC analog chip [1]. The GPD permits space, energy and time resolved polarisation measurements. The intrinsically homogeneous and symmetric response, the simultaneous analysis of all the angles and the negligible background allows for a non-rotating polarimeter, unlike in photoelectric polarimeters based on the Time Projection Chamber techniques. However, to cover a larger band, it is necessary to use two detectors that, inside a single camera (see Fig. 12), can be alternatively located at the focus of one NHXM telescope, by a sliding (or a rotary) device: a low energy polarimeter (LEP) and a medium energy polarimeter (MEP) covering the energy band 2–35 keV [19]. The LEPpermits sensitive imaging spectro-polarimetry in the 2–10 keV energy band. The base-line mixture is He-DME at 1 atm with 1 cm absorption gap. The gas cell is a stack of MACOR frames. The beryllium window (50 μm thick) is capped with a titanium frame. Sealed X-ray polarimeters were built, tested and calibrated with stable performance for many years. It has been successfully vibrated at 11.4 g_{rms}, and thermally and vacuum-thermally tested between −15°C and +45°C. An operating detector was irradiated with 500 MeV/nucl._Fe ions equivalent to 40 years LEO operation without performance degradation. The MEP is similar to the LEP, but for the gas cell filled with a Ar-DME mixture, at pressure of 3 atm and a thickness of 3 cm for an operating range of 6–35 keV. Well tuned with the telescope band, the MEP can perform high-sensitivity, imaging polarimetry of hard X-ray sources, a capability absent in GEMS and IXO. A prototype with a 2 cm cell at 2 atm has already been successfully tested. For the final design we foresee a larger gas cell and Gas Electron Multiplier. The LEP and MEP use the same pixel front-end ASIC. The LEP and MEP sensitivity are provided in Fig. 13.

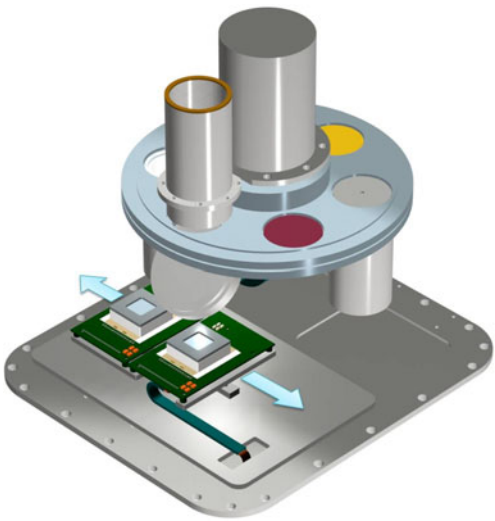

Fig. 12 The polarimetric focal plane camera

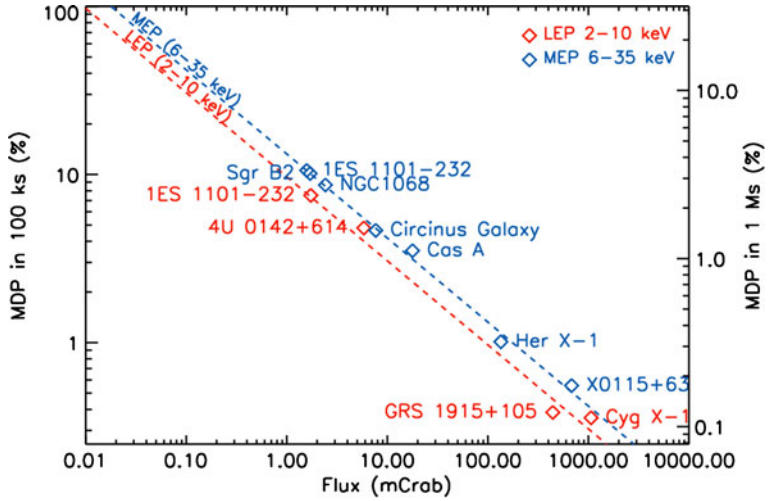

Fig. 13 LEP and MEP minimum detectable polarisation at 99% confidence level. The *dashed lines* are for a Crab-like spectrum

The wide field X-ray monitor The WFXRM is based on the Wide Field Camera Units (WFCU). The combination of two WFCU forms a single Wide Field Camera (WFC), allowing for modular configurations. Our baseline assumes two WFCs located inside the central platform cylinder and co-aligned with the NHXM pointing direction. The addition of another four units would permit full sky coverage (see Fig. 14). A WFCU is formed by a 20 × 20 cm silicon drift detector coupled to a 35 × 35 cm thin Tungsten asymmetric 2-D coded mask 15 cm away from the detector layer providing an angular resolution of 3 arcmin × 1.5° (see Fig. 15). This design is based on the heritage of the X-ray monitor of the Italian mission AGILE, successfully operating since 2007 [6]. In the current WFCU design, the performance is improved by using 450-μm-thick, large-area and multi-linear Silicon Drift Detectors (SDDs, Vacchi et al. [24]), built on the heritage of the ALICE Inner Tracking System operating since 2008 at the LHC at CERN. This instrument is sensitive in the band 2–50 keV with an energy resolution of 250–500 eV FWHM. A thin passive shield prevents photons of the diffuse X-ray background from entering the field of view, acting also as a supporting structure for the coded mask.

5 System requirement and spacecraft key factors

The long focal length (≥10 m) required by the multilayer X-ray optics poses strong constraints on launcher fairing dimension if implemented in a conventional monolithic X-ray observatory (e.g. XMM-Newton and Chandra like). Consequently, since 2004, a new mission class has been envisaged, where the focal length is achieved by means of a deployment mechanism. This is the

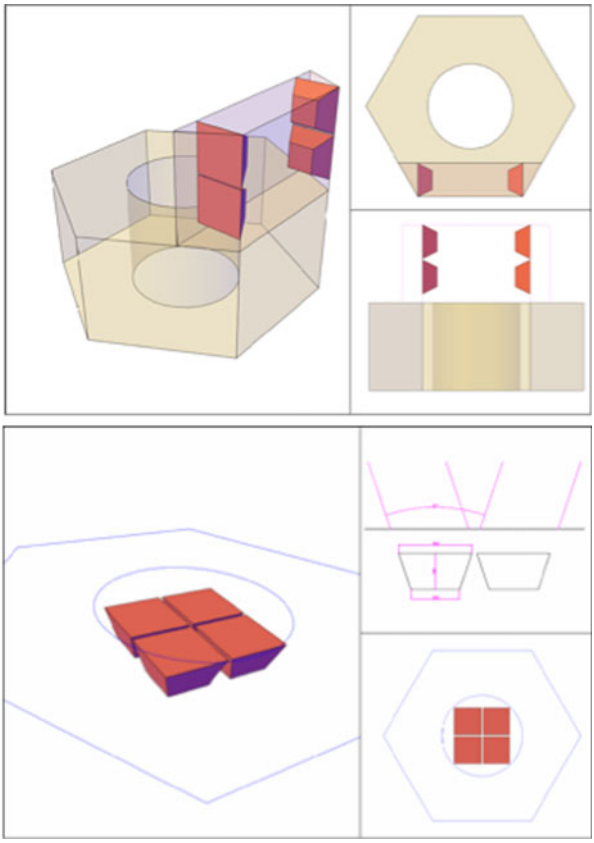

Fig. 14 Location of the WFXRM; *bottom panel* shows the baseline configuration, while the *top panel* shows a possible all-sky configuration

concept of NHXM (also adopted for IXO and before for NuStar and ASTRO-H) studied in detail by ThalesAleniaSpaceItaly. The satellite architecture identified is shown in Fig. 16 and consists of three main elements, i.e.:

- The Instrument Platform that carries the Instruments subsystem.
- The Service Platform that carries the four MM, the WFXRM and all the servicing subsystems.
- The Deployment Mechanism.

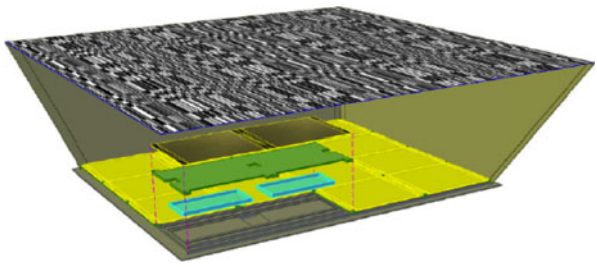

Fig. 15 Configuration of one WFCU

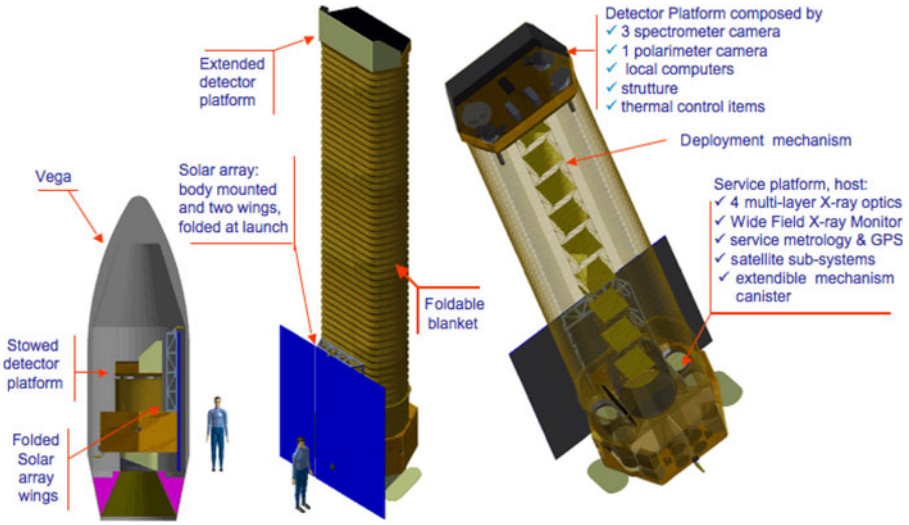

Fig. 16 NHXM in the stowed and deployed position

Soon after injection to orbit and commissioning, the Deployment Mechanism will separate the Instrument Platform from the Service Platform, at the operating distance of telescope focal length. The focal length must not change by more than ± 1 cm and the alignment between the optics reference axis of each of the Mirror Modules and the focal plane reference axis must be stable within 1.5 arcmin. Moreover the Mirror Modules temperature must be stabilised within 1°C along the radius and 2°C along the shells. Consequently, the performance requirements are driven by the system stability over the time scale of an observation and under large temperature gradients, which occur during LEO orbit. As a result of our investigation, the selected Deployment Mechanism, was the ADAM truss, an off-the-shelf lightweight telescopic boom of the ATK company which has good reliability and strong heritage (a similar telescopic boom will be used for the NuSTAR satellite).

The satellite is three axis stabilised, with pointing constraints applied with respect to the Sun (20°), the Earth limb and the Moon (5°). For any pointing direction compatible with these constraints, a rotational degree of freedom, around the long axis of the satellite, is available and is used for thermal and power reasons.

The relative position of the detectors with respect to the associated optics will be monitored by means of an optical metrology system. For each detected photon it will be possible to determine a positional correcting factor. Each event will be also characterised by the detection time measured via the on board GPS.

Analysis of orbital perturbation (drag, gravity gradient, Sun pressure) has shown the mission feasibility for the selected LEO orbit, optimal for the planned science. A detailed trade-off study between scientific requirements,

mass, telemetry and power budgets has shown the compatibility of the mission with the VEGA launcher (see Fig. 16).

We designed the mission to be compatible with an S-Band RF link, with a telemetry down-link rate to the GS of ∼2 Mbps from the Kourou ground station (Malindi can be an alternative). This RF down-link rate sets the on-board data processing capability, the mass memory sizing and the observing strategy. The payload subsystems that in principle will generate most of the telemetry are the WFXRM, if operated in "photon-mode" (i.e. the information is stored and down-linked for every single event), the polarimeters and the CCDs. The WFXRM data will be accumulated, analysed and compressed in "images" recorded on board every 5 minutes. The "photon-mode" acquisition will be activated for 5 min only on specific source triggers. A large amount of telemetry is also generated by the polarimeter when observing bright sources (if we downlink all track information, see payload section). This situation can be accommodated within the downlink capability in two ways: (1) by a dedicated onboard large mass memory (5 GB) and scheduling the observation of weak sources (the majority) after a bright source; (2) by onboard track reconstruction, downlinking only the main photon parameters. A similar situation applies to the CCDs, for which we will adopt the same strategy as for the polarimeters.

The requirement for the NHXM Attitude and Orbit Control (AOC) is the achievement of an HEW$<15''$ (for energies E $\leq$ 10 keV) that has been associated with an Absolute Pointing Error of $15''$ (3σ). We assessed the perturbing actions (perturbing torques) evaluating the sensitivity to atmospheric drag and gravity gradient with simulations. Other perturbation effects (Earth albedo, Earth magnetic field) are less relevant for the AOC design. Based on these studies and considering:

- The launch vehicle injection accuracy compatible with the operative orbit: no additional DeltaV maneuvers;
- Reaction wheel download by magnetic-torque action;
- The acquisition phases assuming a three axis stabilised pointing with Earth magnetic field measurement (carried out by magnetometers) and Sun position (carried out by Sun sensor);
- Magnetometers and Sun sensor for the attitude determination during the momentum management mode (optionally);
- RCS based on hydrazine propulsion to support only the End of Life phase;

We were able to select a standard AOC architecture with equipment well proven in missions familiar to the scientific consortium (BeppoSAX, Swift, AGILE).

For the selected equatorial orbit the VEGA launcher has a mass capability of 2,100 kg (see VEGA User's Manual Issue 3). The total mass of NHXM is of 1,965 kg, including the 20% margin on each subsystem or unit plus the addition of another 20% system level margin. The total power budget request is of 1,286 W, including the 20% margin on each subsystem or unit plus the

addition of another 20% system level margin. Finally the average bandwidth telemetry requirement is of 169 kbps.

6 Conclusions

The NHXM brings together for the first time simultaneous high-sensitivity, hard-X-ray imaging, broadband spectroscopy and polarimetry. With these capabilities the NHXM will perform groundbreaking science in key scientific areas, including:

- Black hole census, cosmic evolution and accretion physics. Accretion onto compact objects is the dominant process producing X-rays in the Universe. The cosmic history of accretion is encoded in the Cosmic X-ray Background (CXB), peaking at 30 keV and mostly produced at $z = 1$–2. Resolving the CXB at its peak will uncover elusive AGN heavily obscured by gas and dust, providing invaluable insight into the interplay between Super Massive Black Hole growth and the evolution of the host galaxies. Polarimetry and broad-band X-ray spectroscopy will provide information on the nature of the AGN primary component and the hard reflection component from circum-nuclear matter.
- Acceleration mechanisms and non-thermal emission. Winds and jets from AGN propagate over extremely long distances (Mpc scales) and can be responsible for significant energy injection into the interstellar matter in galaxies and intra-cluster gas. However, the physics behind the formation of jets and their emission mechanisms remain quite poorly understood. Similarly, cosmic rays are believed to be accelerated in shocks, both in supernova remnants and in the intra-cluster medium. However, the details of shock development and cosmic ray production remain a mystery. Sensitive broadband imaging, spectroscopy and polarimetry can provide breakthroughs on all these problems.
- Physics of matter under extreme conditions. General relativistic effects on emission line profiles and continuum spectra, and on the polarisation properties of the radiation emitted by the accretion disk, can be used to estimate the BH spin, a key parameter for black hole birth and growth. The line and continuum methods already provide results that are often in disagreement, indicating insufficient control of the systematics and underlying continuum. This can be overcome only by broadband, high throughput observations. A third, independent method is to exploit the spin-dependent rotation with energy of the polarisation angle of the disk emission.

To address these scientific goals NHXM will have the following capabilities: broad 0.5–80(120) keV band for imaging and spectroscopy; 15″ HEW angular resolution at 30 keV; sensitivity limits that are >3 orders of magnitude better than those available in present day instruments; broadband (2–35 keV) imaging polarimetry. Moreover, it will be able to locate and actively monitor

sources in different states of activity and to repoint within 1–2 h. The NHXM satellite has been proposed to ESA in response to the Cosmic Vision M3 call. Its configuration and payload subsystems were studied in previous national efforts, leading to a mature configuration compatible with a VEGA launch before 2020.

Acknowledgements The technical part for system, payload accommodation and service platform of the proposal submitted to ESA has been prepared thanks the support of ThalesAleniaSpaceItaly with the contribution from the team involved in the preliminary NHXM studies. This work was supported by ASI Grant I/069/09/0.

References

1. Bellazzini, R., Spandre, G., Minuti, M., et al.: A sealed gas pixel detector for X-ray astronomy. NIMPA **579**, 853 (2007)
2. Bellazzini, R., Brez, A., Minuti, M., et al.: The high-energy detector of the New Hard X-ray Mission (NHXM): design concept. SPIE **7732**, 77323O (2010)
3. Costa, E., Soffitta, P., Bellazzini, R., et al.: An efficient photoelectric X-ray polarimeter for the study of black holes and neutron stars. Nature **411**, 662 (2001)
4. Duncan, R.C., Thompson, C.: Formation of very strongly magnetized neutron stars - implications for gamma-ray bursts. ApJ. **392**, L9 (1992)
5. Fender, R.P., Belloni, T., Gallo, E.: Towards a unified model for black hole X-ray binary jets. MNRAS **355**, 1105 (2004)
6. Feroci, M., Costa, E., Soffitta, P., et al.: SuperAGILE: the hard X-ray imager for the AGILE space mission. NIMPA **581**, 728 (2007)
7. Fiore, F., Grazian, A., Santini, P., et al.: Unveiling obscured accretion in the Chandra deep field-south. ApJ. **672**, 94 (2008)
8. Goosmann, R.W., Matt, G.: Spotting the misaligned outflows in NGC 1068 using X-ray polarimetry. MNRAS (astro-ph: 1012.4652) (2011, in press)
9. Israel, G.L., Romano, P., Mangano, V., et al.: A swift gaze into the 2006 March 29 burst forest of SGR 1900+14. ApJ. **685**, 1114 (2008)
10. Luo, B., Bauer, F.E., Brandt, W.N., et al.: The Chandra deep field-south survey: 2 Ms source catalogs. ApJS. **179**, 19
11. McNamara, A.L., Kuncic, Z., Wu, K.: X-ray polarisation in relativistic jets. MNRAS **395**, 1507 (2009)
12. Mereghetti, S.: The strongest cosmic magnets: soft gamma-ray repeaters and anomalous X-ray pulsars. A&ARev. **15**, 225 (2008)
13. Miller, J.M., Reynolds, C.S., Fabian, A.C., et al.: Stellar-mass black hole spin constraints from disk reflection and continuum modeling. ApJ. **697**, 900 (2009)
14. Pareschi, G., Tagliaferri, G., Attinà, P.: Design and development of the optics system for the NHXM hard x-ray and Polarimetric mission. SPIE **7437**, 743704 (2009)
15. Raban, D., Jaffe, W., Röttgering, H., et al.: Resolving the obscuring torus in NGC 1068 with the power of infrared interferometry: revealing the inner funnel of dust. MNRAS **394**, 1325 (2009)
16. Romaine, S., Boike, J., Bruni, R., et al.: Mandrel replication for hard x-ray optics using titanium nitride. SPIE **7437**, 74370Y (2009)
17. Shafee, R., McClintock, J.E., Narayan, R., et al.: Estimating the spin of Stellar-Mass black holes by spectral fitting of the X-ray continuum. ApJ. **636**, L113 (2006)
18. Schnittman, J.D., Krolik, J.H., X-ray polarisation from accreting black holes: coronal emission. ApJ. **712**, 908 (2010)

19. Soffitta, P., Costa, E., Muleri, F., et al.: A set of x-ray polarimeters for the new hard x-ray imaging and polarimetric mission. SPIE **7732**, 77321A (2010)
20. Tagliaferri, G., Basso, S., Borghi, G., et al.: Simbol-X hard x-ray focusing mirrors: results obtained during the phase a study. AIPC **1126**, 35 (2009)
21. Treister, E., Urry, C.M., Virani, S.: The space density of compton-thick active galactic nucleus and the x-ray background. ApJ. **696**, 110 (2009)
22. Turner, T.J., Miller, L.: X-ray absorption and reflection in active galactic nuclei. A&ARev. **17**, 47 (2009)
23. van Weeren, R.J., Röttgering, H.J., Brüggen, M., Hoeft, M.: Particle acceleration on mega-parsec scales in a merging galaxy cluster. Science **330**, 347 (2010)
24. Vacchi, A., Castoldi, A., Chinnici, S., et al.: Performance of the UA6 large-area silicon drift chamber prototype. NIMPA **306**, 187 (1991)
25. Zoghbi, A., Fabian, A.C., Uttley, P., et al.: Broad iron L line and X-ray reverberation in 1H0707-495. MNRAS **401**, 2419 (2010)